Nonlinear Dynamics (2005) 41: 147–169

The Method of Proper Orthogonal Decomposition for Dynamical Characterization and Order Reduction of Mechanical Systems: An Overview

GAETAN KERSCHEN[1,5,*], JEAN-CLAUDE GOLINVAL[1], ALEXANDER F. VAKAKIS[2,3], and LAWRENCE A. BERGMAN[4]

[1]*Department of Materials, Mechanical and Aerospace Engineering, University of Liège, Liège, Belgium;* [2]*Division of Mechanics, National Technical University of Athens, Athens, Greece;* [3]*Department of Mechanical and Industrial Engineering (adjunct), Department of Aerospace Engineering (adjunct), University of Illinois at Urbana-Champaign, Illinois, U.S.A.;* [4]*Department of Aerospace Engineering, University of Illinois at Urbana-Champaign, Illinois, U.S.A.;* [5]*Present address: Postdoctoral fellow, National Technical University of Athens, Athens, Greece, and the University of Illinois at Urbana-Champaign, Illinois, U.S.A.;* [*]*Author for correspondence (e-mail: g.kerschen@ulg.ac.be; fax: +32-4-3664856)*

(Received: 27 January 2004; accepted: 16 July 2004)

Abstract. Modal analysis is used extensively for understanding the dynamic behavior of structures. However, a major concern for structural dynamicists is that its validity is limited to linear structures. New developments have been proposed in order to examine nonlinear systems, among which the theory based on nonlinear normal modes is indubitably the most appealing. In this paper, a different approach is adopted, and proper orthogonal decomposition is considered. The modes extracted from the decomposition may serve two purposes, namely order reduction by projecting high-dimensional data into a lower-dimensional space and feature extraction by revealing relevant but unexpected structure hidden in the data. The utility of the method for dynamic characterization and order reduction of linear and nonlinear mechanical systems is demonstrated in this study.

Key words: dynamic characterization, order reduction, proper orthogonal decomposition

1. Introduction

The proper orthogonal decomposition (POD) is a multi-variate statistical method that aims at obtaining a compact representation of the data. This method may serve two purposes, namely order reduction by projecting high-dimensional data into a lower-dimensional space and feature extraction by revealing relevant, but unexpected, structure hidden in the data.

The key idea of the POD is to reduce a large number of interdependent variables to a much smaller number of uncorrelated variables while retaining as much as possible of the variation in the original variables. An orthogonal transformation to the basis of the eigenvectors of the sample covariance matrix is performed, and the data are projected onto the subspace spanned by the eigenvectors corresponding to the largest eigenvalues. This transformation decorrelates the signal components and maximizes variance.

The most striking property of the POD is its optimality in the sense that it minimizes the average squared distance between the original signal and its reduced linear representation. Although it is frequently applied to nonlinear problems, it should be borne in mind that the POD only gives the optimal approximating *linear* manifold in the configuration space represented by the data. The linear nature of the method is appealing because the theory of linear operators is available, but it also exhibits its major limitation when the data lie on a nonlinear manifold. As stated in reference [1], the POD is

"*a safe haven in the intimidating world of nonlinearity; although this may not do the physical violence of linearization methods*".

Since POD has begun to be widely used in structural dynamics, it is certainly of interest to provide an overview of the method. The paper is thus organized as follows: In the next section, a literature survey of the applications of the POD is presented. Section 3 recalls its mathematical formulation, whereas the different means of computing the decomposition are explained in Section 4. Section 5 provides some insight into the physical interpretation of the modes extracted from the POD. One possible application of the technique, namely dynamic characterization and order reduction of mechanical systems, is then explained. Finally, the method's strengths as well as its limitations are discussed in the conclusions.

2. Bibliographical and Historical Review

The POD, also known as the Karhunen-Loève decomposition (KLD), was proposed independently by several scientists including Karhunen [2], Kosambi [3], Loève [4], Obukhov [5] and Pougachev [6] and was originally conceived in the framework of continuous second-order processes (see reference [7] for a recent survey). When restricted to a finite dimensional case and truncated after a few terms, the POD is equivalent to principal component analysis (PCA) [8]. This latter methodology originated with the work of Pearson [9] as a means of fitting planes by orthogonal least squares but was also proposed by Hotelling [10]. It is emphasized that the method appears in various guises in the literature and is known by other names depending on the area of application, namely PCA in the statistical literature, empirical orthogonal function in oceanography and meteorology, and factor analysis in psychology and economics. The reader is referred to references [11–15] for a detailed discussion about the equivalence of the POD, PCA and KLD, and their connection with the singular value decomposition (SVD).

Because of the large amount of computations required to find the POD modes, the technique was virtually unused until the middle of the 20th century. Radical changes came with the appearance of powerful computers. The POD has now gained popularity and is being used in numerous fields. For instance, several authors used the POD in the context of turbulence to extract coherent structures (see e.g. reference [16]). Wax and Kailath [17] suggested its use to detect the number of signals in a multichannel time-series. In reference [18] the modes of a reaction-diffusion chemical process are captured by means of the KLD and the dynamic behaviour is ascertained. Bayly et al. [19] employed the KLD to describe quantitative changes in spatial complexity during extended episodes of ventricular fibrillation. Epureanu et al. [20] obtained reduced-order models of unsteady viscous flows. Barnston and Ropelewski [21] employed the method for forecasting in meteorology. Leen et al. [22] introduced it as a means of classifying speech data.

The first applications of the POD in the field of structural dynamics date back to the 1990s. Fitzsimons and Rui [23] considered the method for determining low-dimensional models of distributed systems. Cusumano and co-authors [24, 25] exploited the technique for dimensionality studies. Kreuzer and Kust [26] used the POD for the control of self-excited vibrations of long torsional strings. Azeez and Vakakis [27] applied it to create low-dimensional models of an overhung rotor.

The POD now enjoys various applications in structural dynamics such as active control [28], aeroelastic problems [29, 30], damage detection [31–33], dynamic characterization [34–41], finite element model updating [42, 43], modal analysis [44, 45], multibody systems [46], model order reduction [47–52], sensor validation [53, 54] and stochastic structural dynamics [55–58].

3. Mathematical Formulation

The mathematical formulation of the POD presented here closely follows the one in reference [16]. Let $\theta(x, t)$ be a random field on a domain Ω. This field is first decomposed into mean $\mu(x)$ and time varying parts $\vartheta(x, t)$:

$$\theta(x, t) = \mu(x) + \vartheta(x, t) \tag{1}$$

At time t_k, the system displays a snapshot $\vartheta^k(x) = \vartheta(x, t_k)$. The POD aims at obtaining the most characteristic structure $\varphi(x)$ of an ensemble of snapshots of the field $\vartheta(x, t)$. This is equivalent to finding the basis function $\varphi(x)$ that maximizes the ensemble average of the inner products between $\vartheta^k(x)$ and $\varphi(x)$:

$$\text{Maximize} \quad \langle |(\vartheta^k, \varphi)|^2 \rangle \quad \text{with } \|\varphi\|^2 = 1 \tag{2}$$

where $(f, g) = \int_\Omega f(x)g(x)\, d\Omega$: denotes the inner product in Ω; $\langle \cdot \rangle$: denotes the averaging operation; $\| \cdot \| = (\cdot, \cdot)^{\frac{1}{2}}$: denotes the norm; $| \cdot |$: denotes the modulus.

Expression (2) means that if the field ϑ is projected along φ, the average energy content is greater than if the field is projected along any other basis function.

The constraint $\|\varphi\|^2 = 1$, imposed to make the computation unique, can be taken into account by the use of a Lagrange multiplier:

$$J[\varphi] = \langle |(\vartheta, \varphi)|^2 \rangle - \lambda(\|\varphi\|^2 - 1) \tag{3}$$

The extremum is reached when the functional derivative is equal to zero. Reference [16] shows that this condition reduces to the following integral eigenvalue problem:

$$\int_\Omega \langle \vartheta^k(x)\vartheta^k(x') \rangle \varphi(x')\, dx' = \lambda\varphi(x) \tag{4}$$

where $\langle \vartheta^k(x)\vartheta^k(x') \rangle$ is the averaged auto-correlation function.

The solution of the optimization problem (2) is thus given by the orthogonal eigenfunctions $\varphi_i(x)$ of the integral Equation (4), called the proper orthogonal modes or POD modes (POMs). The corresponding eigenvalues λ_i ($\lambda_i \geq 0$) are the proper orthogonal values (POVs). The POMs may be used as a basis for the decomposition of the field $\vartheta(x, t)$:

$$\vartheta(x, t) = \sum_{i=1}^{\infty} a_i(t)\varphi_i(x) \tag{5}$$

where the coefficients $a_i(t)$ are uncorrelated, i.e., $\langle a_i(t)a_j(t) \rangle = \delta_{ij}\, \lambda_i$, and are determined by $a_i(t) = (\vartheta(x, t), \varphi_i(x))$.

The POM associated with the greatest POV is the optimal vector to characterize the ensemble of snapshots. The POM associated with the second greatest POV is the optimal vector to characterize the ensemble of snapshots but restricted to the space orthogonal to the first POM, and so forth. The energy ϵ contained in the data is defined as the sum of the POVs, i.e., $\epsilon = \sum_j \lambda_j$, and the energy percentage captured by the ith POM is given by $\lambda_i / \sum_j \lambda_j$.

4. Computation of the Proper Orthogonal Decomposition

In practice, the data are discretized in space and time. Accordingly, n observations of a m-dimensional vector $\mathbf{x}$ are collected, and an $(m \times n)$ response matrix is formed:

$$\mathbf{X} = [\mathbf{x}_1 \ \cdots \ \mathbf{x}_n] = \begin{bmatrix} x_{11} & \cdots & x_{1n} \\ \cdots & \cdots & \cdots \\ x_{m1} & \cdots & x_{mn} \end{bmatrix} \tag{6}$$

The purpose of this section is to present several means of computing the POD.

4.1. Eigensolutions of the Sample Covariance Matrix

Since the data are now discretized and do not necessarily have a zero mean, the averaged auto-correlation function is replaced by the covariance matrix $\boldsymbol{\Sigma} = E[(\mathbf{x} - \boldsymbol{\mu})(\mathbf{x} - \boldsymbol{\mu})^{\mathrm{T}}]$, where $E[\cdot]$ is the expectation and $\boldsymbol{\mu} = E[\mathbf{x}]$ is the mean of the vector $\mathbf{x}$. Under the assumption that the process is stationary and ergodic and that the number of time instants is large, a reliable estimate of the covariance matrix is given by the sample covariance matrix:

$$\boldsymbol{\Sigma}_S = \frac{1}{n} \begin{bmatrix} \left\{ \sum_{j=1}^{n} \left(x_{1j} - \frac{1}{n} \sum_{k=1}^{n} x_{1k} \right)^2 \right\} & \cdots & \left\{ \sum_{j=1}^{n} \left(x_{1j} - \frac{1}{n} \sum_{k=1}^{n} x_{1k} \right) \left(x_{mj} - \frac{1}{n} \sum_{k=1}^{n} x_{mk} \right) \right\} \\ \cdots & \cdots & \cdots \\ \left\{ \sum_{j=1}^{n} \left(x_{mj} - \frac{1}{n} \sum_{k=1}^{n} x_{mk} \right) \left(x_{1j} - \frac{1}{n} \sum_{k=1}^{n} x_{1k} \right) \right\} & \cdots & \left\{ \sum_{j=1}^{n} \left(x_{mj} - \frac{1}{n} \sum_{k=1}^{n} x_{mk} \right)^2 \right\} \end{bmatrix} \tag{7}$$

The POMs and POVs are thus characterized by the eigensolutions of the sample covariance matrix $\boldsymbol{\Sigma}_S$. If the data have a zero mean, the sample covariance is merely given by the following expression:

$$\boldsymbol{\Sigma}_S = \frac{1}{n} \mathbf{X}\mathbf{X}^{\mathrm{T}} \tag{8}$$

It should be noted that when the number of degree-of-freedom is much higher than the number of snapshots (e.g., in turbulence theory), the computation of the sample covariance matrix may become expensive. In this context, the POD modes are most easily computed using the method of snapshots proposed by Sirovich in reference [59]. However, the description of this technique is beyond the scope of this paper.

4.1.1. *Interpretation of the Eigenvalue Problem*

If a matrix is real, symmetric and positive definite, then the eigenvectors of the matrix are the principal axes of the associated quadratic form that is an m-dimensional ellipsoid centered at the origin of the

Euclidean space [60]. Accordingly, the POMs, as eigenvectors of the sample covariance matrix $\mathbf{\Sigma}_S$, are the principal axes of the family of ellipsoids defined by:

$$\mathbf{z}^{\mathrm{T}}\mathbf{\Sigma}_S\,\mathbf{z} = c \tag{9}$$

where $\mathbf{z}$ is a real non-zero vector and c is a positive constant.

The result is statistically important if the data have a multi-variate normal distribution. In this case, the ellipsoids given by (9) define contours of constant probability [61].

4.2. Singular Value Decomposition of the Response Matrix

For any real $(m \times n)$ matrix $\mathbf{X}$ (i.e., for our purpose, the response matrix measured about its mean), there exists a real factorization called the singular value decomposition (SVD) that can be written:

$$\mathbf{X} = \mathbf{USV}^{\mathrm{T}} \tag{10}$$

where $\mathbf{U}$ is an $(m \times m)$ orthonormal matrix containing the left singular vectors; $\mathbf{S}$ is an $(m \times n)$ pseudo-diagonal and semi-positive definite matrix with diagonal entries containing the singular values σ_i and $\mathbf{V}$ is an $(n \times n)$ orthonormal matrix containing the right singular vectors.

Reliable algorithms have been developed to compute the SVD [62]. The SVD may also be calculated by means of solving two eigenvalue problems, or even one if only the left or the right singular vectors are required. Indeed,

$$\begin{aligned}\mathbf{XX}^{\mathrm{T}} &= \mathbf{US}^2\mathbf{U}^{\mathrm{T}}\\ \mathbf{X}^{\mathrm{T}}\mathbf{X} &= \mathbf{VS}^2\mathbf{V}^{\mathrm{T}}\end{aligned} \tag{11}$$

According to Equations (11), the singular values of $\mathbf{X}$ are found to be the square roots of the eigenvalues of $\mathbf{XX}^{\mathrm{T}}$ or $\mathbf{X}^{\mathrm{T}}\mathbf{X}$. In addition, the left and right singular vectors of $\mathbf{X}$ are the eigenvectors of $\mathbf{XX}^{\mathrm{T}}$ and $\mathbf{X}^{\mathrm{T}}\mathbf{X}$ respectively. The POMs, defined as the eigenvectors of the sample covariance matrix $\mathbf{\Sigma}_S$ (8), are thus equal to the left singular vectors of $\mathbf{X}$. The POVs, defined as the eigenvalues of matrix $\mathbf{\Sigma}_S$, are the square of the singular values divided by the number of samples m.

The main advantage in considering the SVD to compute the POD instead of the eigenvalue problem described in Section 4.1 is that additional information is obtained through the matrix $\mathbf{V}$. The column $\mathbf{v}_i$ of matrix $\mathbf{V}$ contains the time modulation of the corresponding POM $\mathbf{u}_i$, normalized by the singular value σ_i. This information provides important insight into the system dynamics and plays a prominent role in the model updating of nonlinear systems [43].

4.2.1. *Interpretation of the Singular Value Decomposition*

The SVD of a matrix $\mathbf{X}$, seen as a collection of column vectors, provides important insight into the oriented energy distribution of this set of vectors. It is worth recalling that:

1. The energy of a vector sequence $\mathbf{x}_i$ building an $(n \times m)$ matrix $\mathbf{X}$ is defined via the Frobenius norm:

$$\epsilon(\mathbf{X}) = \|\mathbf{X}\|_F^2 = \sum_{i=1}^{n}\sum_{j=1}^{m} x_{ij}^2 = \sum_{k=1}^{p}\sigma_k^2, \quad \text{where } p = \min(m, n) \tag{12}$$

so that the energy of a vector sequence is equal to the energy in its singular spectrum $\sigma_1^2, \ldots, \sigma_p^2$;

2. The oriented energy of a vector sequence in some direction k with unit vector $\mathbf{e}_k$ is the sum of squared projections of the vectors onto direction k:

$$\epsilon_k(\mathbf{X}) = \sum_{i=1}^{m} \left(\mathbf{e}_k^{\mathrm{T}} \mathbf{x}_i\right)^2 \tag{13}$$

One essential property of SVD is that extrema in this oriented energy distribution occur at each left singular direction [63, 64]. The oriented energy measured in the direction of the kth left singular vector is equal to the kth singular value squared. Since the POMs are equal to the left singular vectors, it can be stated that they are optimal with respect to energy content in a least squares sense; i.e., they capture more energy per mode than any other set of basis functions.

4.3. A Simple Learning Rule

Consider the following simple iterative scheme [65]:

$$\begin{aligned} y &= \mathbf{x}^{\mathrm{T}}\mathbf{w} \\ \Delta\mathbf{w} &= \mathbf{w}_{(j+1)} - \mathbf{w}_{(j)} = \alpha(y_{(j)}\mathbf{x}_{(j)} - {y_{(j)}}^2\mathbf{w}_{(j)}) \end{aligned} \tag{14}$$

where $\mathbf{x}$ is the vector containing the inputs; $\mathbf{w}$ is the vector containing the weights; y is the output; α is the learning rate controlling the speed of convergence; $\ldots_{(j)}$ refers to the result of the jth iteration.

After convergence, the expectation of the weight update $\Delta\mathbf{w}$ is equal to zero:

$$\begin{aligned} E[\Delta\mathbf{w}] &= E[\alpha(y\mathbf{x} - y^2\mathbf{w})] = \alpha E[\mathbf{x}\mathbf{x}^{\mathrm{T}}\mathbf{w} - \mathbf{w}^{\mathrm{T}}\mathbf{x}\mathbf{x}^{\mathrm{T}}\mathbf{w}\mathbf{w}] \\ &= \alpha(\boldsymbol{\Sigma}\mathbf{w} - \mathbf{w}^{\mathrm{T}}\boldsymbol{\Sigma}\mathbf{w}\mathbf{w}) = 0 \end{aligned} \tag{15}$$

and,

$$\boldsymbol{\Sigma}\mathbf{w} = (\mathbf{w}^{\mathrm{T}}\boldsymbol{\Sigma}\mathbf{w})\mathbf{w} = \lambda\mathbf{w} \tag{16}$$

where $\boldsymbol{\Sigma} = E[\mathbf{x}\mathbf{x}^{\mathrm{T}}]$ is the covariance matrix of $\mathbf{x}$ that is assumed to be zero mean. As can be seen from Equation (16), the weights converge to an eigenvector of the covariance matrix; i.e., a POM. In fact, it can be shown that they approach the eigenvector with the largest eigenvalue. Note that this scheme can be generalized in order to extract the first k POMs [66, 67].

4.4. Auto-Associative Neural Networks

Finally, it is also interesting to mention that the POD can be computed using auto-associative neural networks. Auto-associative neural networks are those in which the target output pattern is identical to the input pattern. The aim is thus to approximate, as closely as possible, the input data itself. When used with a hidden layer smaller than the input and output layers, a perfect reconstruction of all input data is generally not possible. However, it can be shown [68] that an auto-associator with linear activation functions performs a compression scheme equivalent to the POD.

To this end, let us consider an auto-associative neural network with a single hidden unit and a linear activation function as shown in Figure 1. The sum of squares error (SSE) function for this network is

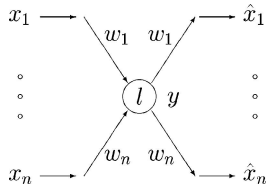

Figure 1. An auto-associative neural network with a single hidden unit with a linear activation function.

given by the following equation:

$$\mathrm{SSE} = \frac{1}{2}(\mathbf{x} - \hat{\mathbf{x}})^{\mathrm{T}}(\mathbf{x} - \hat{\mathbf{x}}) = \frac{1}{2}(\mathbf{x} - y\mathbf{w})^{\mathrm{T}}(\mathbf{x} - y\mathbf{w}) \tag{17}$$

The derivative of the error function is:

$$\frac{\partial(\mathrm{SSE})}{\partial \mathbf{w}} = -\left(\frac{\partial y}{\partial \mathbf{w}}\mathbf{w} + y\frac{\partial \mathbf{w}}{\partial \mathbf{w}}\right)(\mathbf{x} - y\mathbf{w}) = -(\mathbf{x}^{\mathrm{T}}\mathbf{w} + y)(\mathbf{x} - y\mathbf{w}) = -2y(\mathbf{x} - y\mathbf{w}) \tag{18}$$

and the weight update becomes:

$$\Delta\mathbf{w} = -\alpha\frac{\partial(\mathrm{SSE})}{\partial \mathbf{w}} = 2\alpha(y\mathbf{x} - y^2\mathbf{w}) \tag{19}$$

This latter expression is equivalent to learning rule (14) which demonstrates the ability of the auto-associative network to perform the POD.

Although neural networks offer no direct advantage over other means of computing the POD, they suggest an interesting nonlinear generalization referred to as nonlinear principal component analysis [69], which was introduced by Kramer in the chemical engineering literature.

5. Physical Interpretation of the Proper Orthogonal Modes

As shown in the previous section, the POD is directly computed from the system response. The signal-dependent nature of the POD can be seen as one of the weakest points of the method. This prevents us from providing a *general* physical interpretation of the modes extracted from the decomposition.

However, it should be noted that the POMs can bear a resemblance to the physical mode shapes or even coincide with them in some particular cases. The key point is to realize that the POMs are orthogonal to each other, whereas the mode shapes are orthogonal with respect to the mass and stiffness matrices. The rigorous convergence of the POMs to the mode shapes can thus only be obtained for systems whose mass matrix is proportional to the identity matrix.

Apparently, North [70] was the first to establish a formal relationship between the POMs – referred to as empirical orthogonal functions (EOFs) in this study – and the normal modes of mechanical systems. He showed that Hermitian systems excited by a white noise have their EOFs coinciding with their normal modes. The formulation proposed by North allows to consider a broad class of mechanical systems including, for instance, the vorticity equation. In structural dynamics, Cusumano and Bai [24] and Davies and Moon [71] were the first to observe some resemblances between the POMs and the mode shapes; Feeny and Kappagantu [72] then related the POMs to the mode shapes of unforced linear systems. Specifically, they showed that *in the case of free vibrations of an undamped, discrete linear*

system whose mass matrix is proportional to identity, the POMs converge to the mode shapes as the number of samples tends to infinity. Another interesting finding is that, when a system is resonating at a mode, there is no other choice for the dominant POM than to coincide with this mode shape. Note that this is true whatever the mass distribution.

The physical interpretation of the POMs was pursued in references [73–76], and more details have been given in the case of harmonic and random excitations and for continuous structures.

Feeny and Kappagantu [72] also attempted to interpret the POMs of nonlinear systems. However, for nonlinear systems, no general relationships between the POMs and the mode shapes [the nonlinear normal modes (NNMs) in this case] can be drawn. They, however, arrived at the conclusion that, *if the motion is a single, synchronous NNM, the resonant POM minimizes the square of the distance with the NNM under the constraint that it passes through the origin of the co-ordinate system; the POM can therefore be considered as the best linear representation of the NNM.*

Let us illustrate this using the example of a nonlinear, conservative system with two unit masses connected by linear springs k and k_c between two walls, as shown in Figure 2. The first mass is also connected to a wall through a nonlinear spring k_{nl} which behaves according to $f_{nl}(x_1) = k_{nl}\, x_1^3$. For $m = k = 1$, $k_c = k_{nl} = 15$ and initial conditions on the vector displacement $[x_1\ x_2]^{\mathrm{T}}$ equal $[1\ 0.918]^{\mathrm{T}}$, the motion is a single and synchronous NNM; i.e., the displacements are confined to a curve represented in Figure 3a.

The dominant mode given by the POD is shown in Figure 3b together with the synchronous NNM. This figure confirms that this mode can be considered to be the best linear representation of the NNM; it explains 94.29% of the total variance. Also of interest is to represent the amplitude modulation of this identified waveform; i.e., the first column of matrix $\mathbf{V}$ in Equation (10). This is shown in Figure 4. Information about the frequency of oscillation of the mode can then be gleaned by performing a Fourier transform of this signal.

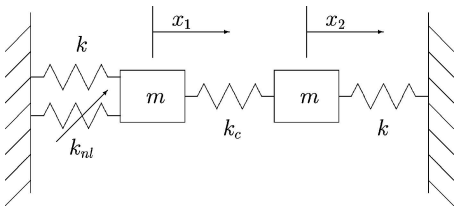

Figure 2. Model of the 2-d.o.f. example.

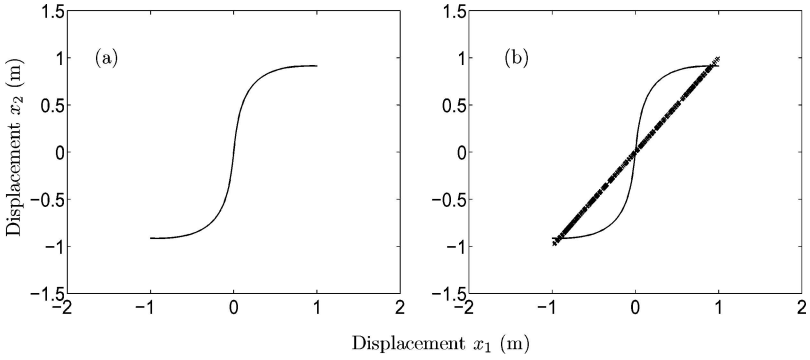

Figure 3. (a) Synchronous NNM motion; (b) Dominant POD mode.

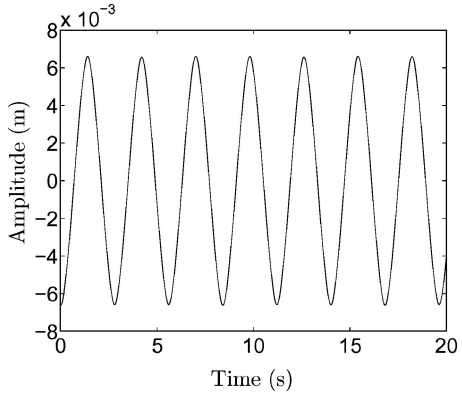

Figure 4. Amplitude modulation of the dominant POM.

6. Dynamic Characterization and Order Reduction of Mechanical Systems

In linear dynamics, the simplest and most popular features for characterizing the structural behavior are the natural frequencies, mode shapes and damping ratios. However, it should be kept in mind that modal analysis is restricted to structures exhibiting linear behavior. New methods have, thus, been proposed to examine nonlinear systems; among them the theory based on nonlinear normal modes [77] is indubitably the most appealing.

The purpose of this section is to show that the POD represents an interesting alternative for the investigation of linear and nonlinear mechanical systems. In the following, we provide applications to problems involving continuous systems.

6.1. Application of the Proper Orthogonal Decomposition to Vibro-Impacting Continuous Systems

In this first application, it will be shown how the POD analysis can be used to study nonlinear dynamical effects in continuous systems due to vibro-impacts. In particular, it will be shown that the POMs and the portion of energy captured by each of the leading (dominant) modes are valuable tools for studying the strength of nonlinear effects in these systems. Indeed, by studying variations and energy redistributions among leading POMs as system parameters change, one can find application to diagnosis of developing defects in structural systems. Hence, the POD method can be an effective non-parametric system identification tool that can be used for diagnosis and monitoring of the performance of vibrating structural assemblies (see also references [31, 32]). In addition, the relative simplicity of the POD calculations facilitates the applicability of the method to a wide class of mechanical systems.

The continuous system considered is the impacting beam depicted in Figure 5. The impacts are assumed to occur at $x = e = 0.5\,\text{m}$, whereas the length of the beam is equal to $L = 0.766\,\text{m}$. The values of e and L will be held fixed for all numerical simulations that follow. The mass per unit length of the beam is $m = 0.735\,\text{kg/m}$, and the product of the modulus of elasticity with the moment of inertia of the beam cross section is $EI = 57.7\,\text{Nm}^2$. This leads to the leading natural frequencies, $\omega_1 = 52.45$, $\omega_2 = 328.73$, $\omega_3 = 920.45\,\text{rad/s}$, and the corresponding modal damping ratios $d_1 = 0.475$, $d_2 = 0.750$ and $d_3 = 0.375\,\text{Ns}^2/\text{m}^2$ (identified through experimental modal analysis of a cantilever beam of identical geometry and material properties). The clearance between the beam and the rigid boundary causing the

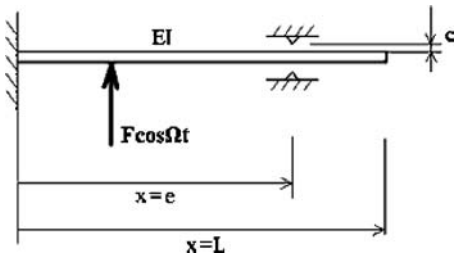

Figure 5. The vibro-impacting beam.

impacts is equal to c, and the system is excited by the harmonic force $F\cos(\Omega t)$, applied at position $x = f$.

The governing partial differential equation is given by:

$$EIu_{xxxx}(x,t) + mu_{tt}(x,t) + du_t(x,t) = \delta(x-f)F\cos(\Omega t) + \delta(x-e)P(u(e,t)) \tag{20}$$

where $u(x,t)$ is the transverse displacement of the beam, $\delta(\bullet)$ is the Dirac delta function, and the term $P(u(e,t))$ represents the concentrated nonlinear force applied to the beam at $x = e$ due to the vibro-impacts; in addition, the short-hand notation for partial differentiation was utilized.

The approximate way of incorporating the vibro-impact terms is to replace the rigid boundary by a stiff spring-damper element; the spring simulates the local compliance of the boundary, and the damper the inelastic impact effects. This scheme is easier to implement computationally, and it enables the direct expression of the vibro-impact term in the equation of motion:

$$P(u(e,t)) = \begin{Bmatrix} K(|u(e,t)| - c)\,\mathrm{sign}(u(e,t)), & |u(e,t)| \geq c \\ 0, & |u(e,t)| < c \end{Bmatrix} \tag{21}$$

where K represents the (high) stiffness of the constraint. Due to its relative simplicity, the approximate method for modeling the vibro-impact effects is adopted in the following simulations. A more detailed discussion of the convergence of the adopted numerical scheme is given in reference [78].

A set of numerical simulations were performed in which the forcing frequency Ω, forcing location f, and the clearance c were varied over a range of values. For each numerical simulation f was fixed and Ω and c were varied. The parameters for the simulations are presented in Table 1, and the forcing function parameters are presented in Table 2. For each case the time series for the snapshots were obtained by

Table 1. Set I: $f = 0.1$ m, $F = 500$ N.

Case no.	1	2	3	4	5	6	7	8	9	10	11	12	13
c (mm)	0	1	2	3	4	5	6	7	8	9	10	20	100

Table 2. Forcing frequency index convention.

Frequency index	1	2	3	4	5	6	7	8	9	10
Ω (rad/s)	30	35	40	45	50	52.4	55	70	80	90
Frequency index	11	12	13	14	15	16	17	18	19	20
Ω (rad/s)	100	110	120	130	140	150	160	170	180	190

integrating the governing partial differential equation of motion; an initial time window of 20 s was discarded to eliminate the transient effects from the response; afterward, data were acquired and stored for post-processing and POD analysis.

It is to be noted that Case 1 represents a clamped-simply supported linear beam (zero clearance), whereas Cases 12 and 13 represent a different linear continuous system, namely a cantilever beam (relatively large clearance for vibro-impacts to occur). The cases between these limiting linear systems represent vibro-impacting beams with strongly nonlinear dynamical effects; it is of interest to study the nonlinear transition between the two limiting linear cases using POD analysis.

The harmonic excitation is applied away from the position of the clearance, and the POMs are sensitive to the clearance parameter c. Indeed, even for small clearance changes, the corresponding POMs show large variations even when the forcing frequency is held constant. Note that there is a propensity for many vibration modes of the beam to be excited due to the vibro-impacts.

When the forcing frequency is low the vibro-impacts are intermittent (relatively small number of impacts), and the POMs are nearly invariant even when the clearance is changed. As the forcing frequency increases the impacts become more frequent, and the deformations of the POMs are more evident.

Of interest is to study the distribution of the energy of the measured time series among the leading POMs for each case, since this provides significant insight into the nonlinear effects due to vibro-impacts. Typical energy distribution diagrams for two cases are depicted in Figure 6, where the energies captured by the three leading POMs are plotted for varying forcing frequencies. By combining all cases one derives the energy distribution surface plots of Figure 7 for varying forcing and clearances. These plots can be used to deduce the strength of the nonlinear effects in the system, and to obtain an approximate dimensionality of the vibro-impact dynamics. Referring to Figure 6a it can be seen that as the forcing frequency increases up to point A profound energy 'transfer' from the first to the second POM takes place, indicating strong nonlinear effects due to vibro-impacts which entails modal coupling and increases of the dimensionality of the dynamics. In the range AB the motion of the beam is sufficiently small so that no vibro-impacts occur; as a result the response of the beam is linear and the first POM capture nearly all the energy of the time series. Increasing the frequency beyond point B the second natural frequency of the beam is approached leading to amplitude increase and vibro-impacts; the induced nonlinearities are manifested by the 'transfer' of energy from the first to the second POM.

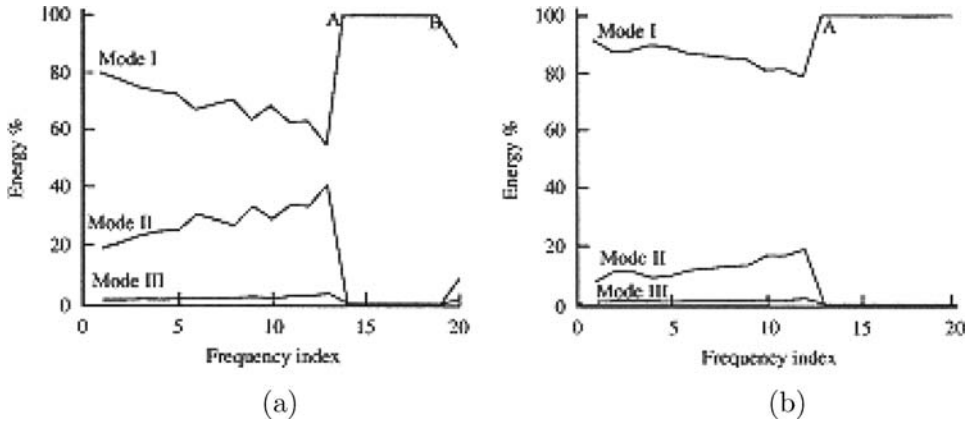

Figure 6. Typical energy distributions among POD modes. (a) Case 6; (b) Case 11.

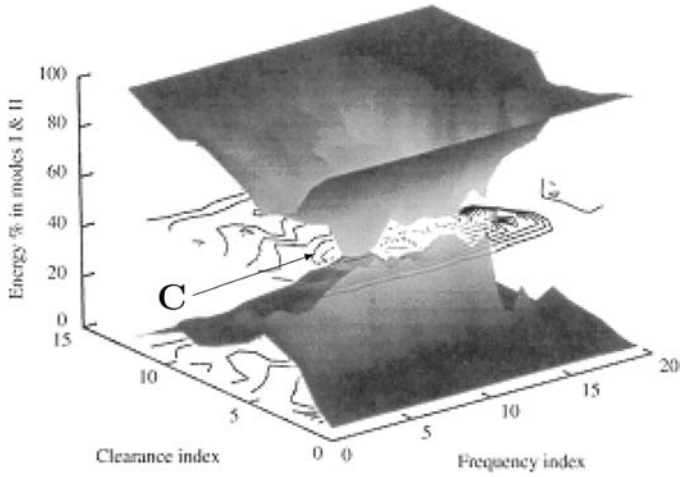

Figure 7. POD energy surface plots.

By examining the surface plots of Figure 7 it is possible to study the nonlinear effects in the system for varying clearance. Indeed, referring to Figure 7, as the clearance index varies between the two limiting linear systems (corresponding to clearance indices 0 and 12 of Set I), there is energy redistribution from the first POM to the second, indicating strong nonlinear effects and increase in the dimensionality of the dynamics. It is of interest to note that there is a point in the plot where 'maximum' nonlinear effects occur, represented by point C in the surface plot; at that point the energy captured by the first (second) POM is minimized (maximized) indicating the furthest departure of the dynamics from linear behavior. Hence, the POD method can be used to study the transition of the dynamics of a system from linear to nonlinear regimes, and to find values of system or excitation parameters where the nonlinear effects are maximized.

A key advantage of obtaining the dominant POMs is that they can be used to construct low-order dynamical models for the system under consideration. For a large-scale structure its response can be simulated using finite-element models employing traditional shape functions. Once a reasonable amount of data is obtained, the POD modes can be extracted from them and low-dimensional models can be constructed. Note that the POD modes extracted from a chaotic orbit can be amazingly effective in capturing the global dynamics of a nonlinear system; the reader is referred to references [48, 79] for numerical studies and to [39–41] for experimental studies. These low-order models can then be used for dynamical studies of structural modifications or for control system design, resulting in large savings in computational effort. This procedure will be referred to as reconstruction and will be applied first to the case of the vibro-impacting beam. To this end, the deformation of the beam in Equation (20) is expressed in the series form:

$$u(x,t) = \sum_{i=1}^{p} \phi_i(x) a_i(t) \tag{22}$$

where only the p-dominant POMs that capture 99.9% of the energy of the analyzed time series are considered.

The POMs $\phi_i(x)$ are used as admissible functions (that satisfy at least the essential boundary conditions), and $a_i(t)$ are the corresponding amplitudes. The POMs are an ideal choice for this

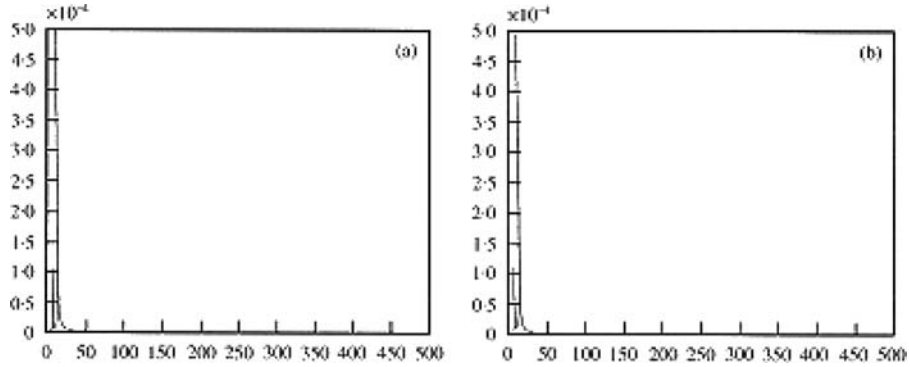

Figure 8. Comparisons of power spectra of the beam responses. (a) Reconstructed; (b) simulated response.

operation, since they satisfy both natural and essential boundary conditions, as well as orthonormality conditions.

Substituting the expansion (22) into (20) and employing the orthogonality condition of the POMs, one obtains the following set of discretized ordinary differential equations:

$$mc_j\ddot{a}_j + dc_j\dot{a}_j + EI\sum_{i=1}^{p}\xi_{ij}a_i = \phi_j(f)F\cos(\Omega t) + P\left(\sum_{i=1}^{p}\phi_i(e)a_i\right)\phi_j(e) \tag{23}$$

where

$$\xi_{ij} = \phi_j(L)\phi_i'''(L) - \phi_j'(L)\phi_i''(L) + \phi_j'(0)\phi_i''(0) + \int_0^L \phi_i''(x)\phi_j''(x)\,\mathrm{dx} \tag{24}$$

Equation (23) is the $2p$-dimensional discretized model of the continuous system, and is integrated numerically by a 4th-order Runge–Kutta algorithm. Details on the routines used can be found in reference [27]. Since the POMs are computed at discrete points in the domain $0 \le x \le L$, interpolations were performed (using B-spline interpolation functions of 6th order) to obtain continuous POMs valid over the entire domain of the computation.

When vibro-impacts are involved it is not always possible to obtain pointwise time domain convergence between the simulated and reconstructed results due to sensitive dependence on initial conditions. In such a situation the responses are transformed and compared in the frequency domain. Such a comparison is shown in Figure 8 for a system with $f = 0.1$ m, $c = 3$ mm, $\Omega = 30$ rad/s, and using only the leading three POMs for the reconstruction. It should be noted that, for continuous systems undergoing vibro-impacts, very small time steps must be used in the numerical integration to get repeatability of the simulations.

6.2. Coherent Spatial Structures in Extended Systems with High Modal Densities

To demonstrate the potential of the POD method to create efficient low-dimensional models of vibrating continuous structures, a second application of the method is given for the dynamical analysis of linear truss dynamics. The main focus of the analysis of this Section is to show that the POD method is capable of effectively reducing the order of the dynamics of spatially extended continuous systems that possess high modal densities, where traditional modal analysis methods are difficult to apply. This

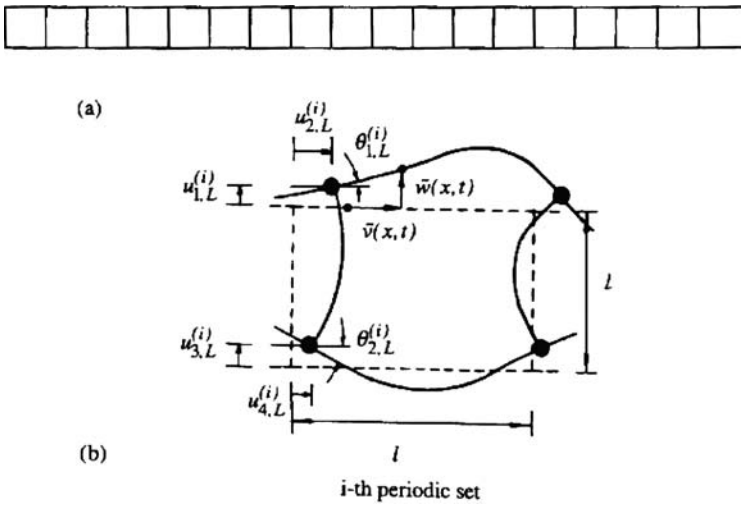

Figure 9. Truss configuration and adopted notation for the displacements and rotations.

type of structure is typical in certain civil engineering and aerospace applications (examples are long construction trusses; lightweight, large-radius circular communication or radar antennas; and the space station which, in essence, is an extended periodic truss with attached modules).

The truss structure considered is shown in Figure 9, consisting of periodic sets (bays) coupled by clamped joints. The analysis will be performed under the assumption of linearity, which is reasonable for this type of spatially extended system. Each periodic set consists of coupled beams undergoing combined axial and bending vibrations. Because the beam vibrations are assumed to be linear, the governing partial differential equations for bending and longitudinal motion of each beam are uncoupled, and coupling and mode conversion between bending and longitudinal vibrations take place through the boundary conditions at the joints. The joints connecting the beams of each periodic set transmit axial and transverse forces, as well as bending moments. Moreover, to simplify the analysis, only in-plane vibrations of the truss are considered, thus rendering the dynamical problem two-dimensional. We consider an 18-bay truss, assuming steady-state harmonic vibration, no structural disorder, and six displacement/rotation coordinates at the boundary of each bay (four axial/transverse displacements and two rotations).

In Figure 10 representative numerical receptance FRFs of the truss are depicted, for vertical external forcing acting on the upper joint of the left boundary. Note that resonances in this system occur in dense clusters which correspond to propagation zones (PZs) of the various families of wavemodes of the corresponding truss of infinite spatial extent; e.g., with an infinite number of bays. It can be shown that the infinite truss possesses six distinct families of wavemodes, with each existing independently of the others, and possessing PZs that overlap in the frequency domain. Depending on the position and direction of the external forcing, truss resonances may correspond to predominantly shear, longitudinal or bending motions, depending on the family of wavemode PZ in which the specific cluster of resonances lies. In addition, mixed-mode resonances may occur, with no obvious truss type of motion, whenever two or more resonance clusters corresponding to different families of wavemodes mix.

POD of the truss dynamics was performed for three distinct loading conditions (LCs) labeled I, II and III, in order to study the dominant coherent structures of the truss under different forcing conditions. In all cases impulsive trapezoidal forces were utilized. LC I corresponds to a single vertical force acting on the upper joint of the left truss boundary. LC II corresponds to a single horizontal force acting on the

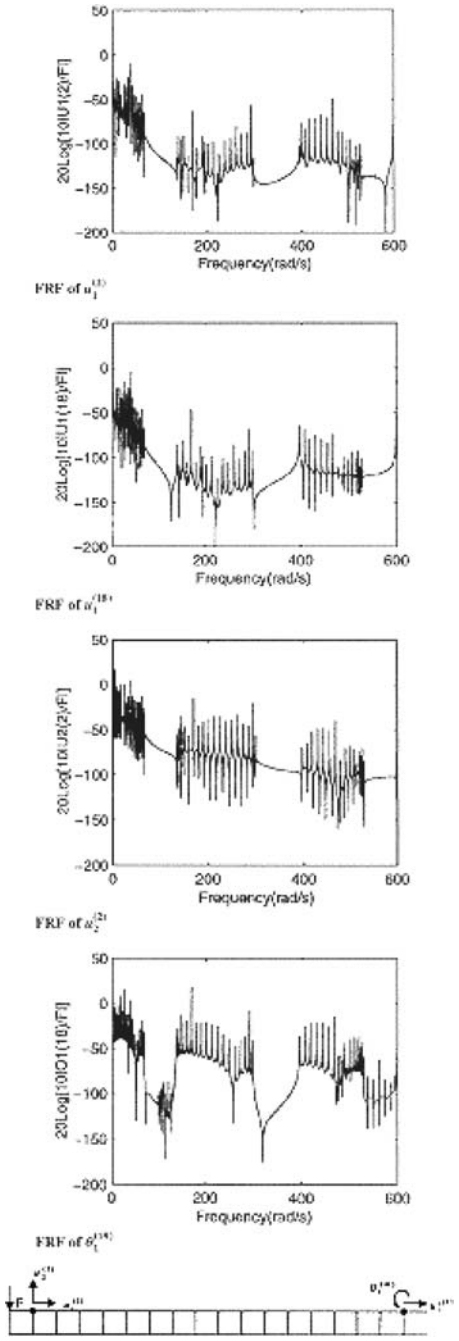

Figure 10. Numerical receptance FRFs of the truss for a vertical external force acting on the upper joint of the left boundary.

same joint of the truss, whereas LC III corresponds to two identical and simultaneous horizontal forces acting on the upper and lower joints of the left truss boundary.

The results of the POD analysis of the truss transient dynamics are depicted in Figures 11–13. The following remarks are made regarding these results. For LC I the truss executes predominantly bending vibrations, and the first three POD modes capture a significant portion of the energy of the truss time

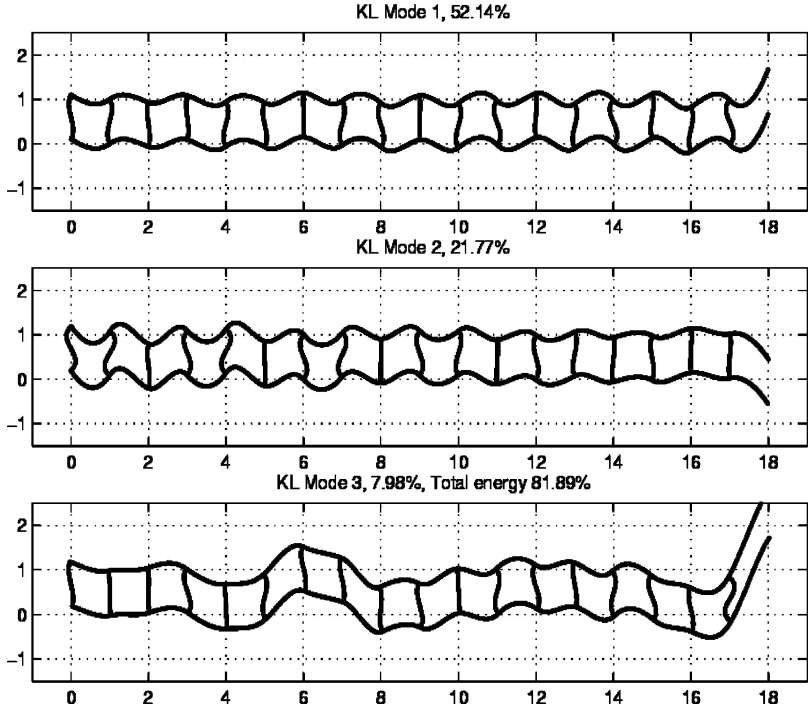

Figure 11. Dominant POD modes for LC I.

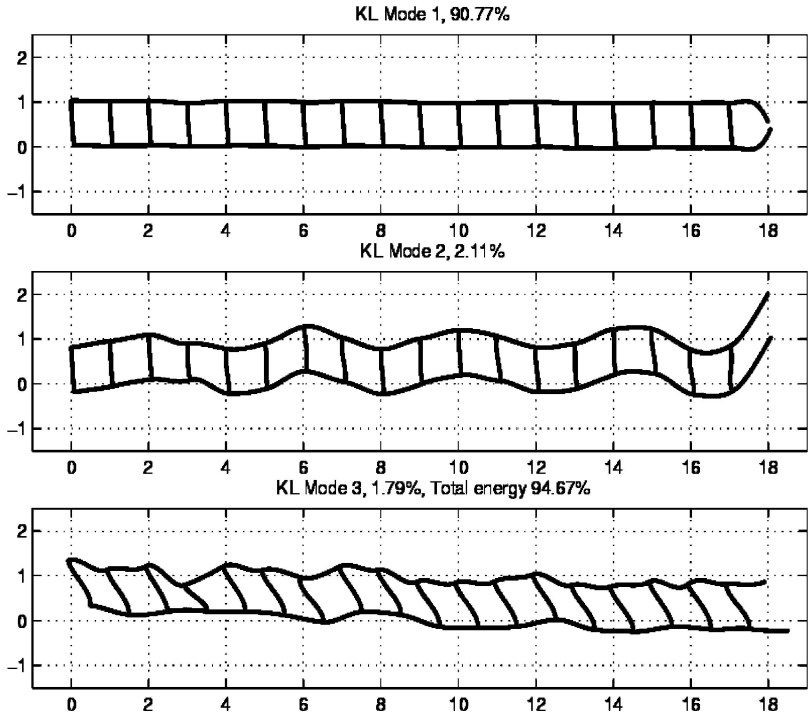

Figure 12. Dominant POD modes for LC II.

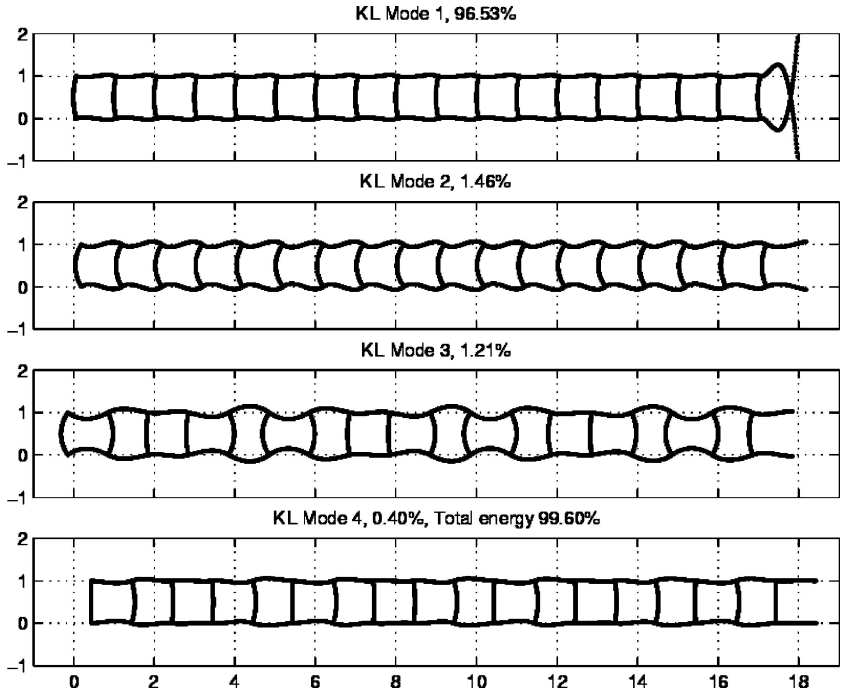

Figure 13. Dominant POD modes for LC III.

series, with the first POD mode capturing a little more than 50% of the total energy. The POD modes involve predominantly vertical motions of the joints; the relatively large displacements of the joints of the right boundary are due to the lack of a vertical longeron there.

When horizontal forces are considered (LCs II and III), there is a qualitative change of the results. In these cases the truss vibrates predominantly in the longitudinal direction, and for each case the leading POMs capture an essential amount of the energy of the truss and dominate all other higher order modes. This is in contrast to what was observed in LC I, where a stronger partition of energy was noted between the leading set of POMs. Hence, it appears that for the case of horizontal forcing most of the energy of the truss is channeled to a single dominant coherent structure (POD mode) that dominates the truss response. This feature is even more noticeable for LC III when two horizontal forces are symmetrically applied on the left boundary of the truss; in this case the dominant POM captures 96.5% of the total energy.

For LC II the forcing is applied unsymmetrically, and the dominant POM corresponds to shear-like deformation of the truss, as one would expect from physical intuition. For LC III, where symmetric forcing is applied, the deformation resembles that due to a pressure wave propagating longitudinally along the truss. An interesting observation is that for LC III the fourth POM resembles a rigid-body deformation of the truss.

It is emphasized that the POMs discussed herein are mathematical modes, describing the spatial coherent structures developing in the truss as energy gets partitioned among the periodic sets of the system for each specific forcing condition. As such, these modes have no resemblance to the classical vibration modes of the truss that one obtains by solving the relevant eigenvalue problem of the dynamics. However, in similarity to vibration mode shapes, the POD modes form a complete orthogonal basis (if all of them are retained), and, hence, they can be used to project the dynamics into low-dimensional

spaces, thus creating low-order models of the truss dynamics. By measuring the energy captured by each mode, one can estimate the number of POMs required for the creation of accurate reduced-order models and, hence, the dimensionality of the truss dynamics. The fact that only a few leading POMs capture nearly all of the energy of the time series indicates that the dynamics can be described by reduced-order models with few degrees-of-freedom, a result that perhaps is unexpected, given that the 18-bay truss under consideration possesses clusters of densely packed resonances and, thus, high modal density.

Modal analysis of extended lightweight continuous systems similar to the one discussed here is a challenging task due to the high modal densities involved. This feature prevents the application of traditional modal analysis methods due to the presence of numerous interacting vibration modes. By not dealing with physical vibration modes, the POD analysis encounters no such limitations and can be effectively used to perform identification on this type of system. Moreover, as mentioned previously for linear systems, the computed POMs are optimal in the sense that they capture more energy of the time series per mode than any other basis of orthogonal modes (including the vibration modes); this optimality feature explains the low-order of the reduced models derived by projecting the truss dynamics into POD bases.

To demonstrate the capability of the POMs to effectively reduce the order of the dynamics of a continuous system, a four-bay truss with free boundary conditions is now considered. Suppose that the POMs of the four-bay truss have already been computed. By construction these modes form an orthogonal basis. In addition, as the number of sensing (measurement) points tends to infinity and covers pointwise the entire truss, the POD basis becomes identical to that formed by the vibration modes of the truss. A discretization of the 24 governing partial differential equations of motion is now performed by projecting the dynamics into a finite-dimensional basis parametrized by the leading p POMs. To this end, the transverse and axial displacements of the k-th elastic member are expressed as (assuming that this member has horizontal undeformed orientation):

$$u_k(x,t) = \sum_{i=1}^{p} \phi_{ki}(x)\, a_i(t), \quad v_k(x,t) = \sum_{i=1}^{p} \psi_{ki}(x)\, a_i(t), \quad k = 1, \ldots, 12 \tag{25}$$

where $a_i(t)$ is the modal amplitude of the i-th POM, and $\phi_{ki}(x)$ and $\psi_{ki}(x)$ are the horizontal and vertical displacement components of the i-th POM for structural member k. The quantities $a_i(t)$ represent global POD modal amplitudes that, for fixed i (mode), are common for all structural members; this definition facilitates significantly the discretization since only p such modal amplitudes need to be defined, instead of defining a separate modal amplitude for each of the twelve structural members. The geometrical and material properties of the four bay truss are as follows: $EA = 2.216 \times 10^6\,\mathrm{Pa\,m^2}$, $EI = 5.587\,\mathrm{Pa\,m^4}$, $m = 0.0555\,\mathrm{kg/m}$, $L_x = L_y = 0.903\,\mathrm{m}$. It is assumed that all structural members have identical material properties, and no structural disorder exists.

Excitation of the truss by a vertical impulsive force $F_{1y}(t) = \delta(t)$ and $F_{1x}(t) = 0$ is considered (cf. Figure 14). In this case the five leading POMs capture 99% of the energy of the time series of the truss. In additional numerical simulations with a finite-time sinusoidal pulse (not reported here; see reference [80]), it was shown that fewer POMs are needed to capture the aforementioned percentage of energy. This indicates that, when impulsive excitation is applied, the energy of the transient dynamics is distributed over POMs of higher order. Reduced-order models of dimensions $m \leq 6$ were considered, and reconstructed transient responses of the truss are shown in Figure 14 using two-, three-, and six-DOF reduced-order models. These are compared to direct numerical simulations. As more DOF are added to the reduced models the reconstructed solutions converge to the direct numerical simulations. It is interesting to note that in this case, a six-DOF reduced model approximates the transient response of a set of 24 coupled partial differential equations of motion (the original continuous model of the four bay truss).

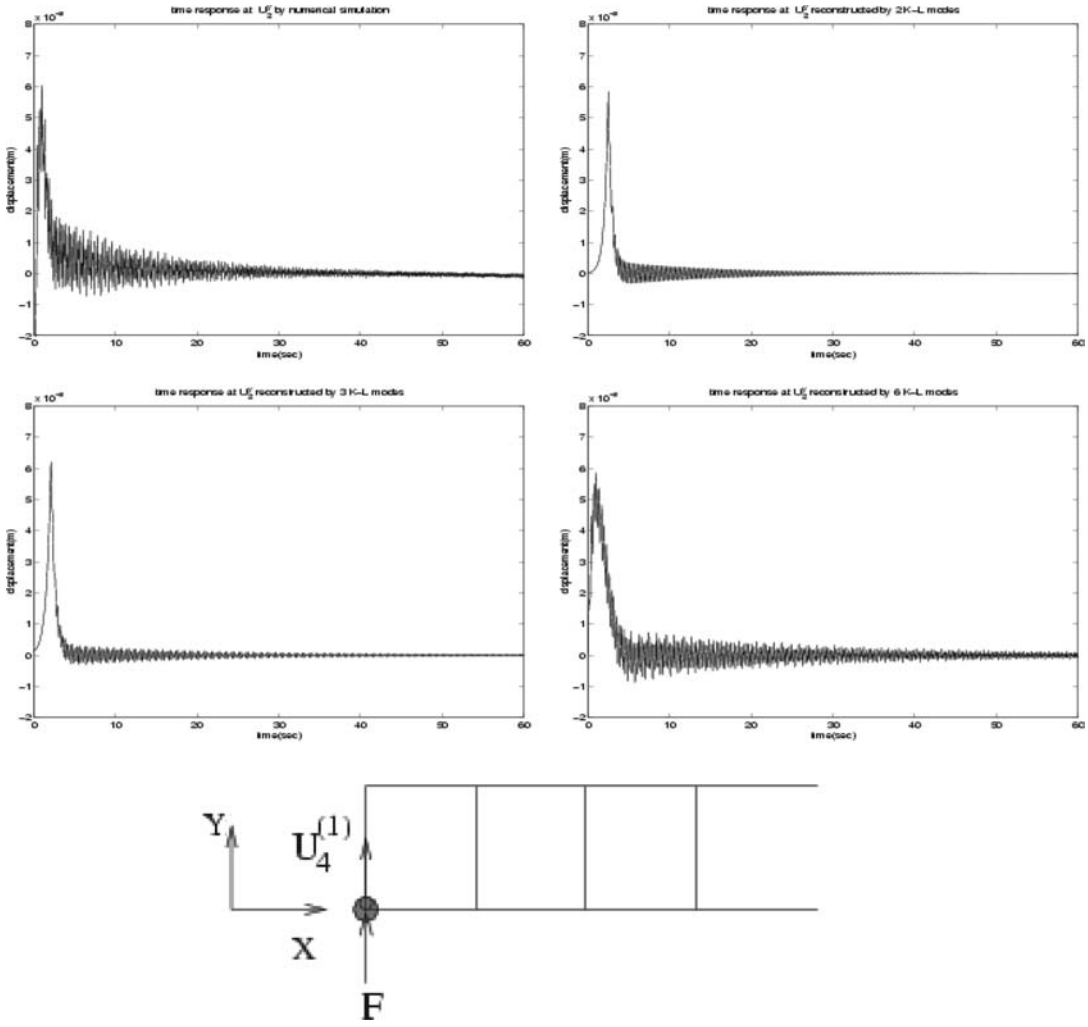

Figure 14. POD-based transient response reconstruction for the displacement $u_4^{(1)}$.

7. Concluding Remarks

The purpose of this paper is to provide an overview of the POD method and to highlight its utility for dynamic characterization and order reduction of linear and nonlinear mechanical systems. We must, however, emphasize that the method can find other applications in structural dynamics such as active control, aeroelasticity, damage detection, finite element model updating, modal analysis, multibody systems, sensor validation and uncertainty modeling.

Indeed, several characteristics of the POD make it very appealing:

– The POMs may be considered as an alternative to the linear mode shapes or the NNMs. Although the POMs do not have the theoretical foundations of those modes, they provide a good characterization of the dynamics. In addition, their computation is straightforward and does not require the knowledge of the structural matrices.
– The POVs give clear indications about the participation of the corresponding POMs in the system response. This enables us to retain only the dominant modes in the analysis and

to filter out the presence of measurement noise which is often associated with the smallest POVs.
- The spatial and time information (contained in matrices **U** and **V**, respectively) is explicitly separated. Insight into the frequency of oscillation of the POMs is thus available.
- If two data sets are to be compared, one can build for both data sets the subspace spanned by the dominant POMs. A useful means of performing the comparison is then to compute the principal angles [81] between the two subspaces. This procedure was not discussed herein but is appealing for damage detection [31, 82] and sensor validation [53, 54], since the current data are to be compared to the reference data, assumed to be healthy.
- Finally, the POD is the optimal linear algorithm since, among all linear techniques, it obtains the minimum expected squared distance between the original signal and its dimension-reduced representation.

Despite its widespread use, the POD may sometimes be too simple for dealing with real-world data. Two weaknesses of the method must be highlighted.

On the one hand, the linear nature of the method may represent a restriction for some data sets. If the data lie on a nonlinear manifold, the method then overestimates the intrinsic dimensionality. For instance, the covariance matrix of data sampled from a helix in $\mathbb{R}^3$ has full-rank, and the POD requires the use of three variables for the description of the data. The helix however is a one-dimensional manifold and can be smoothly parametrized with a single variable. In this case, the method represents the data in a space of higher dimension than the number of intrinsic degrees-of-freedom.

On the other hand, the POD tries to describe all the data using the same global features. Generally, a rich data set often has varying characteristics in different regions of the space. This suggests the use of local features for efficient representation of qualitatively different domains of the data.

The POD can thus determine an appropriate embedding space for a low-dimensional structure, but it cannot provide the most efficient description of a data set where nonlinear dependencies are present. To address this issue, researchers in the field of statistics and neural networks have developed alternatives to the POD that can take nonlinear correlations between the variables into account. Nonlinear principal component analysis (NLPCA) [69] and vector quantization principal component analysis (VQPCA) [83] are possible alternatives. A few attempts to exploit these new techniques in structural dynamics can be found in references [84–87]. Specifically, it was shown in reference [87] that *if the motion of a nonlinear system is a single and synchronous NNM, then the mode given by a NLPCA analysis coincides with this NNM*. This is the generalization of the result of Section 5 in which the dominant POM is found to be the best linear approximation of the NNM.

Finally, it should be emphasized that, since the POD removes linear correlations among variables (i.e. diagonalizes the covariance matrix), it is only sensitive to second-order statistics. Accordingly, it does not necessarily yield statistical independence; decorrelation implies statistical independence only under the assumption that the variables are Gaussian. This limitation has been recently addressed by the introduction of a method called independent component analysis [88] which has begun to be exploited in structural dynamics [89].

Acknowledgements

The first author, G. Kerschen, is supported by grants from the Belgian National Fund for Scientific Research (FNRS) and the Rotary District 1630, which are gratefully acknowledged.

References

1. Berkooz, G., Holmes, P., and Lumley, J. L., 'The proper orthogonal decomposition in the analysis of turbulent flows', *Annual Review of Fluid Mechanics* **25**, 1993, 539–575.
2. Karhunen, K., 'Uber Lineare Methoden in der Wahrscheinlichkeitsrechnung', *Annals of Academic Science Fennicae, Series A1 Mathematics and Physics* **37**, 1946, 3–79.
3. Kosambi, D., 'Statistics in function space', *Journal of Indian Mathematical Society* **7**, 1943, 76–88.
4. Loeve, M., 'Fonctions Aléatoires du Second Ordre', in *Processus stochastiques et mouvement Brownien*, P. Levy (ed.), Gauthier-Villars, Paris, 1948.
5. Obukhov, M. A., 'Statistical description of continuous fields', *Transactions of the Geophysical International Academy Nauk USSR* **24**, 1954, 3–42.
6. Pougachev, V. S., 'General theory of the correlations of random functions', *Izvestiya Akademii Nauk USSR* **17**, 1953, 1401–1402.
7. Berkooz, G., 'Observations on the proper orthogonal decomposition', in *Studies in Turbulence*, Springer, New York, 1992, pp. 229–247.
8. Jolliffe, I. T., *Principal Component Analysis*, Springer, New York, 1986.
9. Pearson, K., 'On lines and planes of closest fit to systems of points in space', *Philosophical Magazine* **2**, 1901, 559–572.
10. Hotelling, H., 'Analysis of a complex of statistical variables into principal components', *Journal of Educational Psychology* **24**, 1933, 417–441, 498–520.
11. Watanabe, S., 'Karhunen-Loève expansion and factor analysis theoretical remarks and applications', in *Proceedings of the 4th Conference on Information Theory*, Prague, Czech Republic, 1965.
12. Mees, A. I., Rapp, P. E., and Jennings, L. S., 'Singular value decomposition and embedding dimension', *Physical Review A* **36**, 1987, 340–346.
13. Ravindra, B., 'Comments on "On the physical interpretation of proper orthogonal modes in vibrations"', *Journal of Sound and Vibration* **219**, 1999, 189–192.
14. Liang, Y. C., Lee, H. P., Lim, S. P., Lin, W. Z., Lee, K. H., and Wu, C. G., 'Proper orthogonal decomposition and its applications, Part I: Theory', *Journal of Sound and Vibration* **252**, 2002, 527–544.
15. Wu, C. G., Liang, Y. C., Lin, W. Z., Lee, H. P., and Lim, S. P., 'A note on equivalence of proper orthogonal decomposition methods', *Journal of Sound and Vibration* **265**, 2003, 1103–1110.
16. Holmes, P., Lumley, J. L., and Berkooz, G., *Turbulence, Coherent Structures, Dynamical Systems and Symmetry*, Cambridge, New York, 1996.
17. Wax, M. and Kailath, T., 'Detection of signals by information theoretic criteria', *IEEE Transactions on Acoustics, Speech and Signal Processing* **33**, 1985, 387–392.
18. Graham, M. D. and Kevrekedis, I. G., 'Alternative approaches to the Karhunen–Loeve decomposition for model reduction and data analysis', *Computers and Chemical Engineering* **20**, 1996, 495–506.
19. Bayly, P. V., Johnson, E. E., Wolf, P. D., Smith, W. M., and Ideker, R. E., 'Predicting patterns of epicardial potentials during ventricular fibrillation', *IEEE Transactions on Biomedical Engineering* **42**, 1995, 898–907.
20. Epureanu, B. I., Hall, K. C., and Dowell, E. H., 'Reduced-order models of unsteady viscous flows in turbomachinery using viscous-inviscid coupling', *Journal of Fluids and Structures* **15**, 2001, 255–273.
21. Barnston, A. G. and Ropelewski, C. F., 'Prediction of ENSO episodes using canonical correlation analysis', *Journal of Climate* **5**, 1992, 1316–1345.
22. Leen, T. K., Rudnick, M., and Hammerstrom, R., 'Hebbian feature discovery improves classifier efficiency', in *Proceedings of the IJCNN, IEEE*, Piscataway, NJ, 1990, pp. 51–56.
23. Fitzsimons, P. M. and Rui, C., 'Determining low dimensional models of distributed systems', in *Advances in Robust and Nonlinear Control Systems*, ASME DSC 53, 1993.
24. Cusumano, J. P. and Bai, B. Y., 'Period-infinity periodic motions, chaos and spatial coherence in a 10-degree-of-freedom impact oscillator', *Chaos, Solitons and Fractals* **3**, 1993, 515–535.
25. Cusumano, J. P., Sharkady, M. T., and Kimble, B. W., 'Experimental measurements of dimensionality and spatial coherence in the dynamics of a flexible-beam impact oscillator', *Philosophical Transactions of the Royal Society of London* **347**, 1994, 421–438.
26. Kreuzer, E. and Kust, O., 'Analysis of long torsional strings by proper orthogonal decomposition', *Archive of Applied Mechanics* **67**, 1996, 68–80.
27. Azeez, M. F. A. and Vakakis, A. F., 'Proper orthogonal decomposition of a class of vibroimpact oscillations', *Journal of Sound and Vibration* **240**, 2001, 859–889.
28. Al-Dmour, A. S. and Mohammad, K. S., 'Active control of flexible structures using principal component analysis in the time domain', *Journal of Sound and Vibration* **253**, 2002, 545–569.
29. Benguedouar, A., 'Proper Orthogonal Decomposition in Dynamical Modeling: A Qualitative Dynamic Approach', PhD thesis, Boston University, Boston, MA, 1995.

30. Epureanu, B. I., Tang, L. S., and Paidoussis, M. P., 'Coherent structures and their influence on the dynamics of aeroelastic panels', *International Journal of Non-Linear Mechanics* **39**, 2004, 977–991.
31. De Boe, P. and Golinval, J. C., 'Principal component analysis of a piezo-sensor array for damage localization', *Structural Health Monitoring* **2**, 2003, 137–152.
32. Feldmann, U., Kreuzer, E., and Pinto, F., 'Dynamic diagnosis of railway tracks by means of the Karhunen–Loève transformation', *Nonlinear Dynamics* **22**, 2000, 183–193.
33. Tumer, I. Y., Wood, K. L., and Busch-Vishniac, I. J., 'Monitoring of signals from manufacturing processes using K-L transform', *Mechanical Systems and Signal Processing* **14**, 2000, 1011–1026.
34. Georgiou, I. T. and Schwartz, I. B., 'Dynamics of large scale coupled structural-mechanical systems: A singular perturbation proper orthogonal decomposition approach', *SIAM Journal of Applied Mathematics* **59**, 1999, 1178–1207.
35. Georgiou, I. T., 'Invariant manifolds, nonclassical normal modes, and proper orthogonal modes in the dynamics of the flexible spherical pendulum', *Nonlinear Dynamics* **25**, 2001, 3–31.
36. Kappagantu, R. and Feeny, B. F., 'Part 1: Dynamical characterization of a frictionally excited beam', *Nonlinear Dynamics* **22**, 2000, 317–333.
37. Kappagantu, R. and Feeny, B. F., 'Part 2: Proper orthogonal modal modeling of a frictionally excited beam', *Nonlinear Dynamics* **23**, 2000, 1–11.
38. Ma, X. and Vakakis, A. F., 'Nonlinear transient localization and beat phenomena due to backlash in a coupled flexible system', *Journal of Vibration and Acoustics* **123**, 2001, 36–44.
39. Alaggio, R. and Rega, G., 'Characterizing bifurcations and classes of motion in the transition to chaos through 3D-Tori of a continuous experimental system in solid mechanics', *Physica D* **137**, 2000, 70–93.
40. Rega, G. and Alaggio, R., 'Spatio-temporal dimensionality in the overall complex dynamics of an experimental cable/mass system', *International Journal of Solids and Structures* **38**, 2001, 2049–2068.
41. Alaggio, R. and Rega, G., 'Exploiting results of experimental nonlinear dynamics for reduced-order modeling of a suspended cable', in *Proceedings of the 18th Biennal Conference on Mechanical Vibration and Noise – ASME DETC*, Pittsburgh, PA, 2001.
42. Hemez, F. M. and Doebling, S. W., 'Review and assessment of model updating for non-linear, transient dynamics', *Mechanical Systems and Signal Processing* **15**, 2001, 45–73.
43. Lenaerts, V., Kerschen, G., and Golinval, J. C., 'Identification of a continuous structure with a geometrical non-linearity, Part II: Proper orthogonal decomposition', *Journal of Sound and Vibration* **262**, 2003, 907–919.
44. Feeny, B. F., 'On proper orthogonal co-ordinates as indicators of modal activity', *Journal of Sound and Vibration* **255**, 2002, 805–817.
45. Han, S. and Feeny, B. F., 'Application of proper orthogonal decomposition to structural vibration analysis', *Mechanical Systems and Signal Processing* **17**, 2003, 989–1001.
46. Quaranta, G., Mantegazza, P., and Masarati, P., 'Assessing the local stability of periodic motions for large multibody non-linear systems using proper orthogonal decomposition', *Journal of Sound and Vibration* **271**, 2004, 1015–1038.
47. Azeez, M. F. A. and Vakakis, A. F., 'Numerical and experimental analysis of a continuous overhang rotor undergoing vibro-impacts', *International Journal of Non-Linear Mechanics* **34**, 1999, 415–435.
48. Kappagantu, R. and Feeny, B. F., 'An optimal modal reduction of a system with frictional excitation', *Journal of Sound and Vibration* **224**, 1999, 863–877.
49. Liang, Y. C., Lin, W. Z., Lee, H. P., Lim, S. P., Lee, K. H., and Sun, H., 'Proper orthogonal decomposition and its applications, Part II: Model reduction for MEMS dynamical analysis', *Journal of Sound and Vibration* **256**, 2002, 515–532.
50. Ma, X., Vakakis, A. F., and Bergman, L. A., 'Karhunen-Loève modes of a truss: Transient response reconstruction and experimental verification', *AIAA Journal* **39**, 2001, 687–696.
51. Ma, X. and Vakakis, A. F., 'Karhunen–Loève decomposition of the transient dynamics of a multibay truss', *AIAA Journal* **37**, 1999, 939–946.
52. Steindl, A. and Troger, H., 'Methods for dimension reduction and their application in nonlinear dynamics', *International Journal of Solids and Structures* **38**, 2001, 2131–2147.
53. Friswell, M. and Inman, D. J., 'Sensor validation for smart structures', *Journal of Intelligent Material Systems and Structures* **10**, 1999, 973–982.
54. Kerschen, G., De Boe, P., Golinval, J. C., and Worden, K., 'Sensor validation using principal component analysis', *Smart Materials and Structures* **14**, 2005, 36–42.
55. Ghanem, R. and Spanos, P., *Stochastic Finite Elements: A Spectral Approach*, Springer, Heidelberg, Germany, 1991.
56. Li, R. and Ghanem, R., 'Adaptive polynomial chaos expansions applied to statistics of extremes in nonlinear random vibration', *Probabilistic Engineering Mechanics* **13**, 1998, 125–136.
57. Sarkar, A. and Ghanem, R., 'Mid-frequency structural dynamics with parameter uncertainty', *Computer Methods in Applied Mechanics and Engineering* **191**, 2002, 5499–5513.
58. Schenk, C. A. and Schueller, G. I., 'Buckling analysis of cylindrical shells with random geometric imperfections', *International Journal of Non-Linear Mechanics* **38**, 2003, 1119–1132.

59. Sirovich, L., 'Turbulence and the dynamics of coherent structures, Part I: Coherent structures', *Quarterly of Applied Mathematics* **45**, 1987, 561–571.
60. Meirovitch, L., *Computational Methods in Structural Dynamics*, Sijthoff and Noordhoff, Alphen a/d Rijn, The Netherlands, 1980.
61. Morrison, D. F., *Multivariate Statistical Methods*, McGraw-Hill, New York, 1967.
62. Golub, G. H. and Van Loan, C. F., *Matrix Computations*, The Johns Hopkins University Press, London, 1996.
63. Otte, D., 'Development and Evaluation of Singular Value Analysis Methodologies for Studying Multivariate Noise and Vibration Problems', PhD thesis, Katholieke Universiteit Leuven, Belgium, 1994.
64. Staar, J., 'Concepts for Reliable Modeling of Linear Systems With Application to On-Line Identification of Multivariate State Space Descriptions', PhD thesis, Katholieke Universiteit Leuven, Belgium, 1982.
65. Oja, E., 'A simplified neuron model as a principal component analyzer', *Journal of Mathematical Biology* **15**, 1982, 267–273.
66. Oja, E., 'Neural networks, principal components and subspaces', *International Journal of Neural Systems* **1**, 1989, 61–68.
67. Sanger, T. D., 'Optimal unsupervised learning in a single linear feedforward neural network', *Neural Networks* **2**, 1989, 459–473.
68. Baldi, P. and Hornik, K., 'Neural networks and principal component analysis: Learning from examples without local minima', *Neural Networks* **2**, 1989, 53–58.
69. Kramer, M. A., 'Nonlinear principal component analysis using autoassociative neural networks', *AIChE Journal* **37**, 1991, 233–243.
70. North, G. R., 'Empirical orthogonal functions and normal modes', *Journal of the Atmospheric Sciences* **41**, 1984, 879–887.
71. Davies, M. A. and Moon, F. C., 'Solitons, chaos and modal interactions in periodic structures', in *Nonlinear Dynamics: The Richard Rand 50th Anniversary Volume*, World Scientific, Singapore, 1997.
72. Feeny, B. F. and Kappagantu, R., 'On the physical interpretation of proper orthogonal modes in vibrations', *Journal of Sound and Vibration* **211**, 1998, 607–616.
73. Feeny, B. F., 'On the proper orthogonal modes and normal modes of continuous vibration systems', *Journal of Vibration and Acoustics* **124**, 2002, 157–160.
74. Feeny, B. F. and Liang, Y., 'Interpreting proper orthogonal modes of randomly excited vibration systems', *Journal of Sound and Vibration* **265**, 2003, 953–966.
75. Kerschen, G. and Golinval, J. C., 'Physical interpretation of the proper orthogonal modes using the singular value decomposition', *Journal of Sound and Vibration* **249**, 2002, 849–865.
76. Lin, W. Z., Lee, K. H., Lu, P., Lim, S. P., and Liang, Y. C., 'The relationship between eigenfunctions of Karhunen-Loève decomposition and the modes of distributed parameter vibration system', *Journal of Sound and Vibration* **252**, 2002, 527–544.
77. Vakakis, A. F., Manevitch, L. I., Mikhlin, Y. V., Pilipchuk, V. N., and Zevin, A. A., *Normal Modes and Localization in Nonlinear Systems*, Wiley, New York, 1996.
78. Emaci, E., Azeez M. A. F., and Vakakis, A. F., 'Dynamics of trusses: Numerical and experimental results', *Journal of Sound and Vibration* **214**, 1998, 953–964.
79. Kerschen, G., Feeny, B. F., and Golinval, J. C., 'On the exploitation of chaos to build reduced-order models', *Computer Methods in Applied Mechanics and Engineering* **192**, 2003, 1785–1795.
80. Ma, X., 'Order Reduction, Identification and Localization Studies of Dynamical Systems', PhD thesis, University of Illinois at Urbana-Champaign, Urbana, IL, 2000.
81. Jordan, C., 'Essai sur la géométrie à n dimensions', *Bulletin de la Société mathématique* **3**, 1875, 103–174.
82. De Cock, K., *Principal Angles in System Theory, Information Theory and Signal Processing*, PhD thesis, Katholieke Universiteit Leuven, Belgium, 2002.
83. Kambhatla, N., 'Local Models and Gaussian Mixture Models for Statistical Data Processing', PhD thesis, Oregon Graduate Institute of Science & Technology, OR, 1996.
84. Sohn, H., Worden, K., and Farrar, C. R., 'Statistical damage classification under changing environmental and operational conditions', *Journal of Intelligent Material Systems and Structures* **13**, 2002, 561–574.
85. Kerschen, G. and Golinval, J. C., 'Non-linear generalisation of principal component analysis: From a global to a local approach', *Journal of Sound and Vibration* **254**, 2002, 867–876.
86. Kerschen, G. and Golinval, J. C., 'A model updating strategy of non-linear vibrating structures', *International Journal for Numerical Methods in Engineering* **60**, 2004.
87. Kerschen, G. and Golinval, J. C., 'Feature extraction using auto-associative neural networks', *Smart Materials and Structures* **13**, 2004, 211–219.
88. Hyvarinen, A., Karhunen, J., and Oja, E., *Independent Component Analysis*, Wiley, New York, 2001.
89. Roan, M. J., Erling, J. G., and Sibul, L. H., 'A new, non-linear, adaptive, blind source separation approach to gear tooth failure detection and analysis', *Mechanical Systems and Signal Processing* **16**, 2002, 719–740.